

Autophagic dysfunction in patients with Papillon-Lefèvre syndrome is restored by recombinant cathepsin C treatment



Pedro Bullón, MD, PhD,^{a,b*} Beatriz Castejón-Vega, BSc,^{a*} Lourdes Román-Malo, PhD,^{a,b} María Paz Jimenez-Guerrero, BSc,^c David Cotán, PhD,^c Tamara Y. Forbes-Hernandez, PhD,^d Alfonso Varela-López, PhD,^e Antonio J. Pérez-Pulido, PhD,^f Francesca Giampieri, PhD,^d José L. Quiles, PhD,^e Maurizio Battino, PhD,^d José A. Sánchez-Alcázar, MD, PhD,^c and Mario D. Cordero, PhD^e *Seville and Armilla, Spain, and Ancona, Italy*

Background: Cathepsin C (CatC) is a lysosomal enzyme involved in activation of serine proteases from immune and inflammatory cells. Several loss-of-function mutations in the CatC gene have been shown to be the genetic mark of Papillon-Lefèvre syndrome (PLS), a rare autosomal recessive disease characterized by severe early-onset periodontitis, palmoplantar hyperkeratosis, and increased susceptibility to infections. Deficiencies or dysfunction in other cathepsin family proteins, such as cathepsin B or D, have been associated with autophagic and lysosomal disorders.

Objectives: Here we characterized the basis for autophagic dysfunction in patients with PLS by analyzing skin fibroblasts derived from patients with several mutations in the CatC gene and reduced enzymatic activity.

Methods: Skin fibroblasts were isolated from patients with PLS assessed by using genetic analysis. Autophagic flux dysfunction was evaluated by examining accumulation of p62/SQSTM1 and a bafilomycin assay. Ultrastructural analysis further confirmed abnormal accumulation of autophagic vesicles in mutant cells. A recombinant CatC protein was produced by a baculovirus system in insect cell cultures.

Results: Mutant fibroblasts from patients with PLS showed alterations in oxidative/antioxidative status, reduced oxygen consumption, and a marked autophagic dysfunction associated with autophagosome accumulation. These alterations were accompanied by lysosomal permeabilization, cathepsin

B release, and NLR family pyrin domain containing 3 (NLRP3) inflammasome activation. Treatment of mutant fibroblasts with recombinant CatC improved cell growth and autophagic flux and partially restored lysosomal permeabilization.

Conclusions: Our data provide a novel molecular mechanism underlying PLS. Impaired autophagy caused by insufficient lysosomal function might represent a new therapeutic target for PLS. (*J Allergy Clin Immunol* 2018;142:1131-43.)

Key words: *Papillon-Lefèvre syndrome, cathepsin C, autophagy, lysosomal permeabilization*

Papillon-Lefèvre syndrome (PLS) is a rare autosomal recessive condition characterized by severe early-onset periodontitis and palmoplantar hyperkeratosis and resulting in premature loss of both deciduous and permanent dentition.¹ Dermatologic symptoms in patients with PLS begin before 2 years of age and continue throughout life.² About 20% to 25% of patients with PLS report increased susceptibility to infections, such as furunculosis and pyoderma, or pyogenic liver abscesses among other complications.² PLS results from mutations that inactivate or introduce loss of function in the cathepsin C (CatC) gene, which are associated with the lack of lysosomal serine protease activities,³ hyperactive neutrophils,¹ increased oxidative stress,² and decreased neutrophil extracellular trap capacity (a relevant defensive mechanism against infectious diseases).⁴

CatC is a lysosomal enzyme involved in processing of certain lysosomal cathepsins and degradation of intracellular proteins.⁵ CatC was also shown to activate several chymotrypsin-like serine proteases by removing an inhibitory N-terminal dipeptide. Cathepsin G; neutrophil elastase; proteinase-3; granzymes A, B, and C; and mast cell chymase tryptase and chymase all require CatC-mediated cleavage for full activation.⁶

The correct cellular turnover of proteins and organelles requires cooperation between both autophagy machinery and lysosomal degradation, a process in which the fusion of autophagosomes with lysosomes has a central role.⁷ As a pathologic process, it is known that accumulation of undegraded substrates in autophagolysosomes caused by lysosomal enzyme deficiency leads to severe pathologic alterations.⁸ This is the main molecular mechanism underlying a set of pathologic conditions known as lysosomal storage diseases, such as Gaucher or Niemann-Pick diseases.⁹

Although the link between CatC and autophagy has not been examined previously, it is reasonable to infer that reduced CatC activity could induce intracellular accumulation of undegraded substrates or dysfunctional organelles similar to other defects detected in family members of the cysteine protease, such as

From ^athe Research Laboratory and ^bthe Department of Periodontology, Dental School, University of Sevilla, Seville; ^cCentro Andaluz de Biología del Desarrollo (CABD), and Centro de Investigación Biomédica en Red: Enfermedades Raras, Instituto de Salud Carlos III, Consejo Superior de Investigaciones Científicas, Universidad Pablo de Olavide, Seville; ^dDipartimento di Scienze Cliniche Specialistiche ed Odontostomatologiche, Sez. Biochimica, Università Politecnica delle Marche, Ancona; ^ethe Department of Physiology, Institute of Nutrition and Food Technology “José Mataix,” Biomedical Research Center (CIBM), University of Granada, Armilla; and ^fCentro Andaluz de Biología del Desarrollo (CABD), Universidad Pablo de Olavide-CSIC-Junta de Andalucía, Seville.

*These authors contributed equally to this work.

Supported by Proyecto de Investigación de Excelencia de la Junta de Andalucía CTS113 and grant PI16/00786, Instituto de Salud Carlos III, Spain, and Fondo Europeo de Desarrollo Regional (FEDER-Unión Europea). In memoriam of Dr Ognjen Culic.

Disclosure of potential conflict of interest: The authors declare that they have no relevant conflicts of interest.

Received for publication September 6, 2017; revised January 11, 2018; accepted for publication January 20, 2018.

Available online February 2, 2018.

Corresponding author: Mario D. Cordero, PhD, Institute of Nutrition and Food Technology “José Mataix Verdú”, Department of Physiology, Biomedical Research Center, University of Granada, 18100 Granada, Spain. E-mail: mdcormor@ugr.es.

The CrossMark symbol notifies online readers when updates have been made to the article such as errata or minor corrections

0091-6749/\$36.00

© 2018 American Academy of Allergy, Asthma & Immunology

<https://doi.org/10.1016/j.jaci.2018.01.018>

Abbreviations used

BafA1:	Bafilomycin A1
CatB:	Cathepsin B
CatC:	Cathepsin C
2,4-DNP:	2,4-Dinitrophenol
LAMP-1:	Lysosomal-associated membrane protein 1
LC3:	Microtubule-associated protein 1A/1B-light chain 3
LMP:	Lysosome/autophagolysosome membrane permeabilization
NLRP3:	NLR family pyrin domain containing 3
OCR:	Oxygen consumption rate
PLS:	Papillon-Lefèvre syndrome
rCatC:	Recombinant cathepsin C
ROS:	Reactive oxygen species

cathepsin B (CatB) deficiency.¹⁰ In the present study we show that fibroblasts derived from patients with PLS presented increased p62/SQSTM1 expression levels and autophagosome accumulation, suggesting impaired autophagic flux. These results were confirmed by biochemical and ultrastructural assays. Increased levels of the mature form of CatB were also observed, as was lysosomal permeabilization. Treatment of mutant fibroblasts derived from patients with PLS with recombinant CatC (rCatC) showed partial recovery of cellular pathologic alterations.

METHODS**Ethical statements**

Approval of the ethics committee of the University of Seville was obtained, according to the principles of the Declaration of Helsinki and the International Conferences on Harmonization and Good Clinical Practice Guidelines. All the participants in the study provided written informed consent before initiating it.

Reagents

Trypsin and bafilomycin A1 (BafA1) were purchased from Sigma Chemical (St Louis, Mo). Anti-glyceraldehyde-3-phosphate dehydrogenase mAb was from Calbiochem-Merck Chemicals (Nottingham, United Kingdom). Anti-NLR family pyrin domain containing 3 (NLRP3) and IL-1 β antibodies were from AdipoGen (San Diego, Calif) and from Santa Cruz Biotechnology, respectively. Anti-active caspase-1, microtubule-associated protein 1A/1B-light chain 3 (LC3), autophagy-related 12 (ATG12), p62, lysosomal-associated membrane protein 1 (LAMP-1), CatB, and galectin-3 were obtained from Cell Signaling Technology (Danvers, Mass). A cocktail of protease inhibitors (complete cocktail) was purchased from Boehringer Mannheim (Indianapolis, Ind). Grace insect medium was purchased from Gibco (Carlsbad, Calif). The Immun-Star HRP Substrate Kit was from Bio-Rad Laboratories (Hercules, Calif).

Fibroblast cultures

Fibroblasts from patients and control subjects were obtained according to the Helsinki Declarations of 1964, as revised in 2001. Two lines of control fibroblasts were used and represented by the mean of both compared with the different patients. Fibroblasts were cultured in high-glucose Dulbecco modified Eagle medium (Gibco, Invitrogen, Eugene, Ore) supplemented with 10% FBS (Gibco, Invitrogen) and antibiotics (Sigma Chemical). Cells were incubated at 37°C in a 5% CO₂ atmosphere.

Structural mutation analysis

The 3-dimensional structure of CatC (UniProt no. P53634) was obtained from the Protein Data Bank database by using the identifier 2DJG, which

has the native structure of human CatC at high resolution and includes only a monomer of the molecule. The structure was visualized with the RasMol program. The functional annotations of the protein, including amino acids corresponding to the active site, were obtained from the well-curated database UniProt.

Enzymatic activity of CatC

CatC activity was determined by measuring the amount of 7-amino-4-methyl coumarin released by means of hydrolysis of a specific substrate (glycyl-L-arginine-7-amido-4-methylcoumarin; Bachem, St Helens, United Kingdom; www.bachem.com) on incubation with sonicated peripheral blood leukocytes, as described previously.¹¹

Antioxidant enzyme activity

Enzymatic activity of antioxidants was determined in 1×10^6 cells. Catalase activity was determined in cellular lysates by monitoring H₂O₂ decomposition at 240 nm.¹² Superoxide dismutase activity was determined based on inhibition of the formation of NADH-phenazine methosulfate-nitroblue tetrazolium formazan.¹³

Western blotting for mitochondrial protein

Whole cellular lysate from fibroblasts was prepared by means of gentle shaking with a buffer containing 0.9% NaCl, 20 mmol/L Tris-ClH (pH 7.6), 0.1% triton X-100, 1 mmol/L phenylmethylsulfonyl fluoride, and 0.01% leupeptin. Protein content was determined by using the Bradford method. Electrophoresis was carried out in 10% to 15% acrylamide SDS-PAGE, and proteins were transferred to Immobilon membranes (Amersham Pharmacia, Piscataway, NJ). Next, membranes were washed with PBS, blocked overnight at 4°C, and incubated with the respective primary antibody solution (1:1000). Membranes were then probed with their respective secondary antibodies (1:2500). Immunolabeled proteins were detected by using a chemiluminescence method (Immun-Star HRP Substrate Kit, Bio-Rad Laboratories). Western blot images were quantified by using ImageJ software (National Institutes of Health, Bethesda, Md; <http://rsb.info.nih.gov/ij/download.html>).

Mitochondrial reactive oxygen species production

Mitochondrial reactive oxygen species (ROS) generation in fibroblasts was assessed by using MitoSOX Red (Thermo Fisher Scientific, Waltham, Mass), a red mitochondrial superoxide indicator. MitoSOX Red is a novel fluorogenic dye developed recently and validated for highly selective detection of superoxide in the mitochondria of live cells. MitoSOX Red reagent is live-cell permeant and rapidly and selectively targeted to the mitochondria. Once in the mitochondria, MitoSOX Red reagent is oxidized by superoxide and exhibits red fluorescence.

Flow cytometry

Approximately 1×10^6 cells were incubated with 1 μ mol/L MitoSOX red for 30 minutes at 37°C, washed twice with PBS, resuspended in 500 μ L of PBS, and analyzed by using flow cytometry in an Epics XL cytometer (Beckman Coulter, Brea, Calif; excitation at 510 nm and fluorescence detection at 580 nm).

Intracellular ROS production

Intracellular ROS levels were determined by using the probe CellROX Orange reagent (Invitrogen, Life Technologies, Milan, Italy), according to the manufacturer's instructions. Briefly, on the first day of the assay, cells were seeded in a 6-well plate at a density of 1.5×10^5 cells/well and allowed to adhere for 16 to 18 hours. Cells were treated with CellROX Orange Reagent, which was added to 1 mL of complete medium at a 1:500 (vol/vol) dilution. Samples were incubated for 30 minutes at 37°C, centrifuged at 320g once to

remove medium and excess dye, and then resuspended in PBS. After labeling with CellROX Orange Reagent, cells were analyzed with the Tali Image-Based Cytometer (Invitrogen, Life Technologies), collecting 20 fields per sample. Control cells were used to determine baseline levels of intracellular ROS and to set the fluorescence threshold for the Tali instrument. Each treatment was carried out in 3 replicates, and the final results were expressed as fold increase compared with control values.

Oxygen consumption rate

Oxygen consumption rate (OCR) was assessed in real time by using the Extracellular Flux Analyzer XF-24 (Seahorse Bioscience, North Billerica, Mass), according to the manufacturer's protocol, which allows measurement of OCR changes after injecting up to 4 different compounds (stimulators, inhibitors, or substrates) affecting bioenergetics. Cells were seeded at a density of 5×10^4 cells/well into the XF-24 cell-culture microplate with complete growth medium and then incubated for 24 hours. Before starting measurements, cells were placed in running Dulbecco modified Eagle medium (supplemented with 25 mmol/L glucose, 2 mmol/L glutamine, and 1 mmol/L sodium pyruvate without serum) and preincubated for 20 minutes at 37°C in the absence of CO₂ in the XF Prep Station Incubator (Seahorse Bioscience). Cells were transferred to the XF-24 Extracellular Flux Analyzer, and after an OCR baseline measurement, profiling of mitochondrial function was performed by means of sequential injection of the following compounds: oligomycin (final concentration, 2.5 µg/mL) at injection in port A, 2,4-dinitrophenol (2,4-DNP; final concentration, 1 mmol/L) at injection in port B, and antimycin/rotenone (final concentration, 10 µmol/L per 1 µmol/L) at injection in port C. A minimum of 5 wells were used per condition in any given experiment. Data are expressed as picomoles of oxygen consumed per minute normalized to 1000 cells (picomoles of oxygen per 1000 cells per minute).

Electron microscopy

Fibroblasts were fixed for 15 minutes in culture plates with 1.5% glutaraldehyde in culture medium and then for 30 minutes in 1.5% glutaraldehyde–0.1 mol/L sodium cacodylate/HCl (pH 7.4). They were then washed 3 times in 0.1 mol/L sodium cacodylate/HCl, pH 7.4, for 10 minutes and postfixed with 1% OsO₄-H₂O, pH 7.4, for 30 minutes. After dehydration in increasing concentrations of ethanol (5 minutes for each step: 50%, 70%, 90%, and 3 times at 100%), impregnation steps and inclusion were performed in Epon and finally polymerized at 60°C for 48 hours. Sixty- to 80-nm sections were obtained by using an ultramicrotome Leica Ultracut S (Leitz Microsystems, Wetzlar, Germany) and contrasted with uranyl acetate and lead citrate. Observations were performed on a Zeiss LEO 906 E (Zeiss, Oberkochen, Germany) transmission electron microscope.

Proliferation rate

Two hundred thousand fibroblasts were cultured in the absence or presence of rCatC (0.25 µg) for 24, 48, 72, and 120 hours. After discharging supernatants with dead cells, cell counting was performed from 3 high-power fields by using an inverted microscope and a $\times 40$ objective.

CatB release

CatB redistribution from lysosomes/autophagolysosomes to the cytosol was assessed by using immunofluorescence techniques with antibodies against CatB and LAMP-1 as a marker of the lysosomal/autophagolysosomal compartment. In control fibroblasts CatB-specific immunostaining revealed cytoplasmic puncta structures surrounded by lysosomal/autophagolysosomal membrane proteins, such as LAMP-1. After lysosomal permeabilization, immunofluorescence detection of CatB reveals a diffuse staining throughout the entire cell.

Galectin 3 puncta

Lysosomal permeabilization was also detected by using the galectin puncta assay, as previously described.¹⁴

rCatC production

The sequence to our rCatC was designed from the literature, and an external service (GeneArt, Invitrogen) was used for its synthesis inside a bacterial vector with ampicillin resistance gene. Construct codifying for rCatC was synthesized and cloned into a pBAC4x baculovirus transfer vector under control of the polyhedrin promoter. The Sf21 cell line was cotransfected by using a linearized modified *Autographa californica* nuclear polyhedrosis viral DNA, and the created transfer plasmid was transferred through a lipofectamin-mediated method, as specified by the manufacturer (Invitrogen). Sf21 cells were sown in 6-well plates (1×10^6 cells/plate). After attachment, cells were infected with the recombinant baculovirus at a multiplicity of infection of 5 for 72 hours at 27°C in the dark. Based on titration of virus obtained by using quantitative PCR and the amount of virus required, volumes were calculated to infect cells. Infected cells and culture supernatants were harvested and separated by means of centrifugation at 800g for 5 minutes at 4°C. The cell pellet was homogenized in $1 \times$ PBS and protease inhibitor at 1 mmol/L phenylmethylsulfonyl fluoride and then sonicated with an ultrasonic processor (Sonopuls HD2070; Bandelin, Berlin, Germany) for 3×10 seconds at 30% potency. Once the clarified fractions were obtained by means of centrifugation with recombinant proteins, these were used in cell-culture assays.

Statistical analysis

Data in the figures are presented as means \pm SDs. Data between different groups were analyzed statistically by using ANOVA on ranks with SigmaPlot and SigmaStat statistical software (SPSS for Windows 19; SPSS, Chicago, Ill). For cell-culture studies, the Student *t* test was used for data analyses. A *P* value of less than .05 was considered significant.

RESULTS

Genetic characterization of patients with PLS showed homozygous and heterozygous mutations in the CatC gene

Three patients were selected for this study. Patient 1 was a 31-year-old man with hyperkeratosis in the palmoplantar region of his hands and moderate periodontitis (Fig 1, A). Genetic characterization revealed that the patient was a compound heterozygote for 2 nonsense cathepsin C (*CTSC*) mutations (c.96T>G and c.401G>A, corresponding to amino acid positions p.Y32* and p.W134*, respectively, and resulting in a premature stop codon, see the [Methods](#) section in this article's Online Repository at www.jacionline.org). The first mutation has been previously described,¹⁵ and the second is a novel mutation. Both genetic changes were observed in the mother and father, respectively, without phenotypic manifestation, whereas the brother did not present with any mutation.

Patient 2 was a 21-year-old woman with hyperkeratosis in the palmoplantar region and joints and moderate periodontitis (Fig 1, B). Genetic characterization showed that the patient was a homozygote for a nonsense *CTSC* mutation, c.1286G>A, corresponding to amino acid position p.W429,* and resulting in a premature stop codon (see the [Methods](#) section in this article's Online Repository). This mutation has been described previously.¹⁶ This genetic change was observed in the mother and father in heterozygosis without phenotypic manifestation, whereas the brother did not show any mutation.

Patient 3 was a 41-year-old woman harboring a previously described mutation (homozygote for a point deletion, c1140delC, corresponding to amino acid position p.S381TTKRGSTTTLV* and resulting in a premature stop codon, see the [Methods](#) section in this article's Online Repository).² The patient presented with hyperkeratosis in the palmoplantar region of the elbows and hands and had severe periodontitis that led to edentulism.

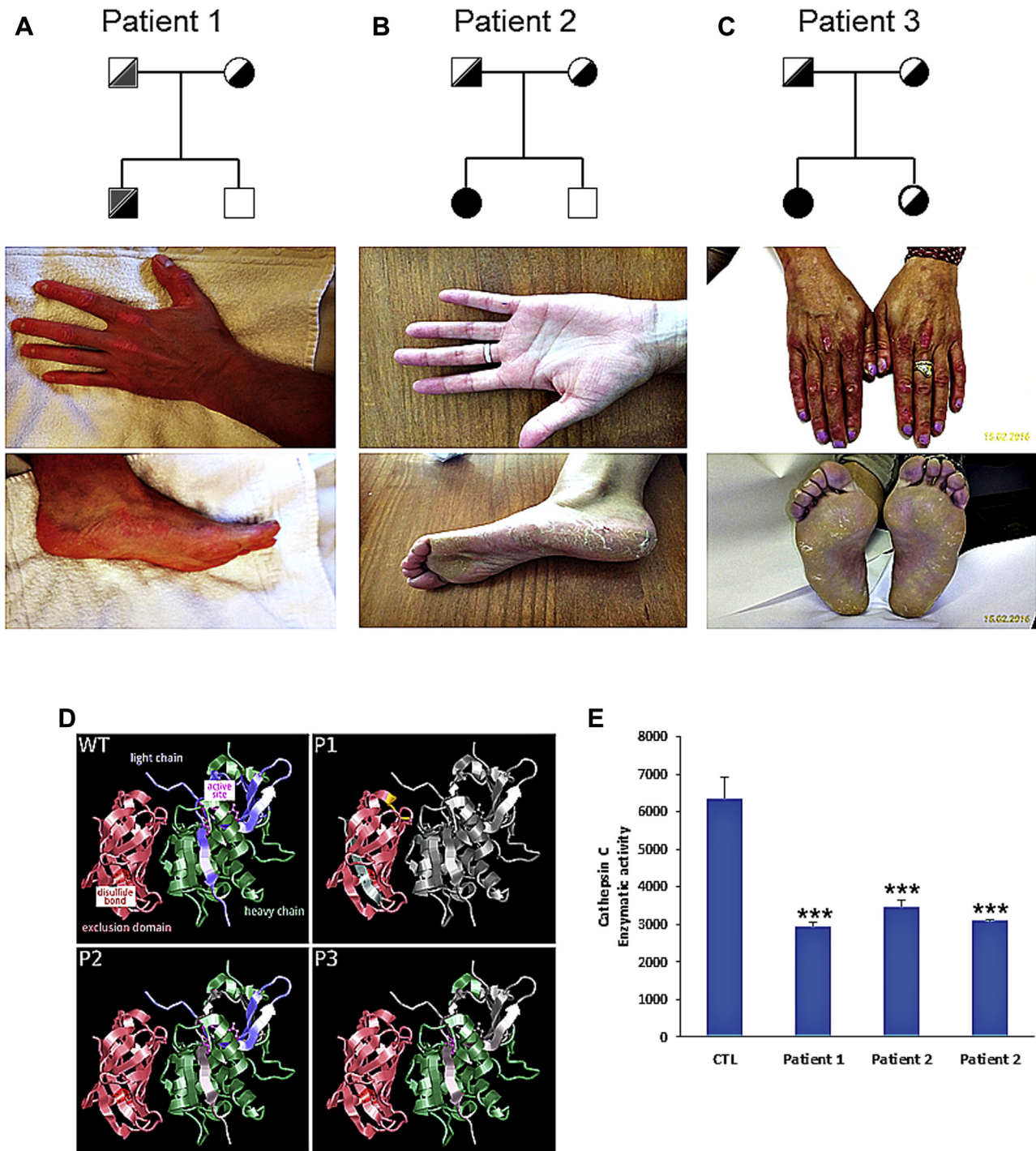


FIG 1. A-C, Pedigree analysis and clinical characteristic of the patients. *Black* or *gray* symbols denote patients with different mutations. *Symbols with two colors* denote 2 heteroplasmic mutations. *Squares*, Men; *circles*, women. **D**, Three-dimensional structure of a CatC monomer. The protein is processed into a proteolytically mature active enzyme consisting of 3 chains: an exclusion domain (flesh color), a heavy chain (green color), and a light chain (violet color). *WT*, Canonical structure highlighting a disulfide bond keeping the folding of the exclusion domain and the 3 amino acids of the active site (pink color). *P1*, Patient 1. The short sequence colored in orange corresponds to 1 allele, and the region colored in gray corresponds to the lost sequence of the other allele. Note that one of the cysteines of the disulfide bond is lost, and it could affect the 3-dimensional structure of the exclusion domain. *P2*, Patient 2. The region colored in gray corresponds to the lost sequence in the mutant. Note that amino acids in the active site are all conserved. *P3*, Patient 3. The region colored in gray corresponds to the lost sequence in the mutant. Note that only 1 amino acid in the active site is conserved. **E**, Enzymatic activity of CatC in homogenates from skin fibroblasts. For control cells, data are means \pm SDs for experiments conducted on 2 different control cell lines. Data represent mean - SDs of 3 separate experiments. *** $P < .001$ between control subjects and patients with PLS.

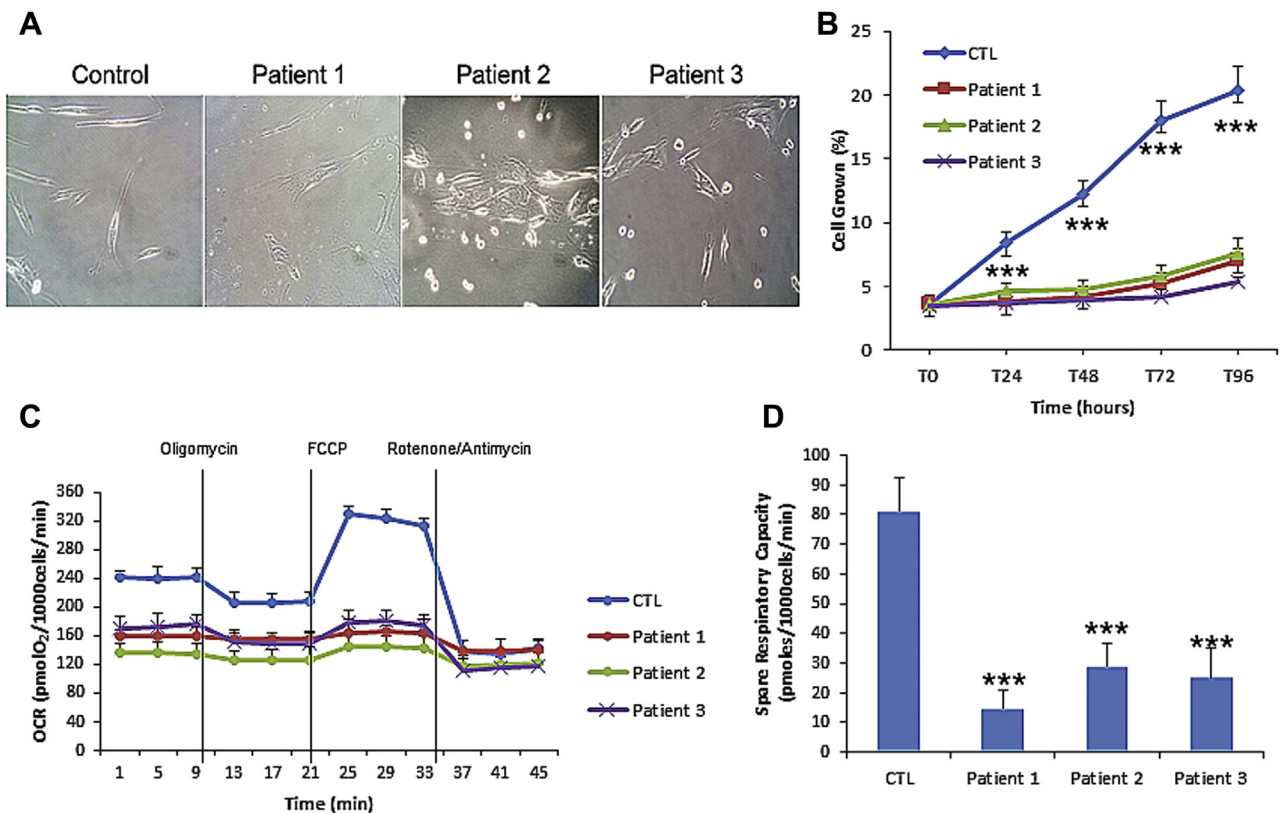


FIG 2. Abnormalities in various aspects of bioenergetic function. **A**, Morphologic changes of fibroblasts from patients compared with control subjects. **B**, Cell growth determined in fibroblasts from healthy control subjects and patients with PLS. **C**, OCR in cells from healthy control subjects and patients with PLS. OCR was monitored by using the Seahorse XF-24 Extracellular Flux Analyzer, with sequential injection of oligomycin (2.5 μ g/mL), 2,4-DNP (1 mmol/L), and antimycin (10 μ mol/L)/rotenone (1 μ mol/L) at the indicated time points. **D**, Spare respiratory capacity of PLS fibroblasts showed a significant decrease compared with control fibroblasts. For control cells, data are mean \pm SDs for experiments conducted on 2 different control cell lines. Data represent mean \pm SDs of 3 separate experiments. *** P < .001 between control subjects and patients with PLS.

The human CatC sequence is processed into a mature form and produces a trimer consisting of the exclusion domain, heavy chain, and light chain, which are bound by disulfide bonds. The active enzyme is composed by a tetramer of these heterotrimers (Fig 1, D, WT). Evaluation of the effect of the amino acid changes on the protein structure of CatC showed the region (colored in gray) corresponding to the lost sequence of the protease. In patient 1 one of the cysteines of the disulfide bond was lost, affecting the 3-dimensional structure of the exclusion domain with important consequences on enzyme function (Fig 1, D, P1). In patient 2 the amino acids in the active site are all conserved. However, according to the protein folding of the light and heavy chains, the mutation might influence the 3-dimensional structure of the enzyme, hence inducing a possible defect on enzyme activity (Fig 1, D, P2). In patient 3 only 1 amino acid in the active site is conserved, and consequently, enzymatic activity is likely affected (Fig 1, D, P3). In agreement with these structural alterations, enzymatic activities of CatC were reduced in all 3 cell lines of mutant fibroblasts (Fig 1, E).

Fibroblasts derived from patients with PLS show metabolic alterations

Given that dermatologic symptoms are relevant clinical manifestations of PLS, fibroblast cell-culture models could

provide information about the molecular mechanisms underlying pathologic alterations in the skin. First, we evaluated the metabolic status of mutant fibroblasts. Fibroblasts from patients with PLS showed reduced growth rates and abnormal morphology (Fig 2, A and B).

We next investigated mitochondrial function by measuring OCR values in fibroblasts from control subjects and patients with PLS. For this, fibroblasts were exposed sequentially to 4 modulators of oxidative phosphorylation: oligomycin (an inhibitor of F_1F_0 -ATPase or complex V), 2,4-DNP (uncoupling of the oxidative phosphorylation electron transport chain), and antimycin/rotenone (complex I and III inhibitors, respectively; Fig 2, C). The basal OCR was affected markedly in fibroblasts from patients with PLS compared with control subjects (Fig 2, C). The spare respiratory capacity of cells, an indicator of how close a cell is operating to its bioenergetics limit, was obtained by calculating the mean of OCR values after injection of 2,4-DNP minus basal respiration. Fibroblasts from patients with PLS showed a significant decrease in spare respiratory capacity compared with control cells (Fig 2, D). These metabolic alterations were accompanied by increased oxidative stress characterized by high levels of ROS and mitochondrial superoxide production and reduced activity of the antioxidant enzymes superoxide dismutase and catalase (see Fig E1 in this article's Online Repository at www.jacionline.org).

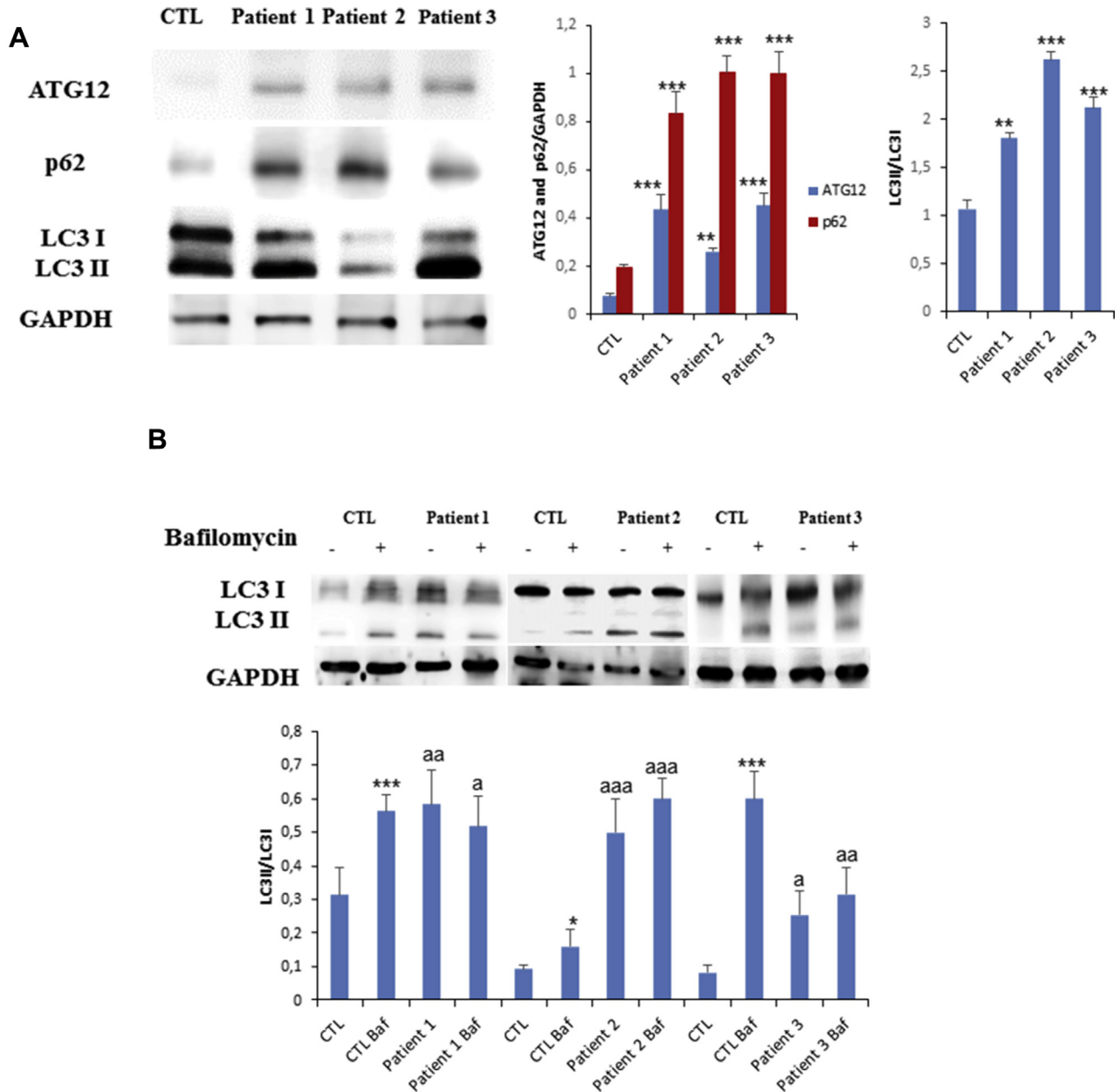


FIG 3. A, Autophagic protein expression levels of ATG12, LC3-I (top panels, top band), LC3-II (top panels, bottom band), and p62 were determined in fibroblast cultures from healthy control subjects and patients with PLS by using Western blot analysis, as described in the Methods section. The ATG12 band represents the Atg12-Atg5 conjugated form. Glyceraldehyde-3-phosphate dehydrogenase (*GAPDH*) was used as a loading control. Data represent the mean - SD of 3 separate experiments. * $P < .05$; ** $P < .01$; *** $P < .001$ between control and patients. **B**, Impaired autophagic flux in fibroblasts from patients with PLS. Determination of LC3-II in the presence and absence of BafA1 in fibroblasts from control subjects (*CTL*) and patients with PLS (*patients*). Fibroblasts from healthy control subjects and patients with PLS were incubated with BafA1 (100 nmol/L for 12 hours). Total cellular extracts were analyzed by means of immunoblotting with antibodies against LC3. *GAPDH* was used as a loading control. For control cells, data are a pool of 2 different control cell lines. Data represent the mean - SD of 3 separate experiments. * $P < .05$; ** $P < .01$; *** $P < .001$ between CTL and CTL+Baf; ^a $P < .05$; ^{aa} $P < .01$; ^{aaa} $P < .001$ between patient and patient+Baf respect to CTL.

Autophagic flux is impaired in fibroblasts from patients with PLS

Because mutant CatC can affect the degradative process during autophagy,¹⁷ we next evaluated expression levels of key proteins involved in autophagy using Western blotting. Expression levels of ATG12 and the autophagy marker LC3-II were markedly increased in fibroblasts from

patients with PLS (Fig 3, A). Furthermore, fibroblasts from patients with PLS showed high expression levels of the polyubiquitin-binding protein p62/SQSTM1, a marker to assess autophagic flux (Fig 3, A).

Next, autophagic flux was also examined through treatment of cells with BafA1, a specific inhibitor of vacuolar H⁺-ATPases and a blocker of autophagosome-lysosome fusion. As expected, BafA1

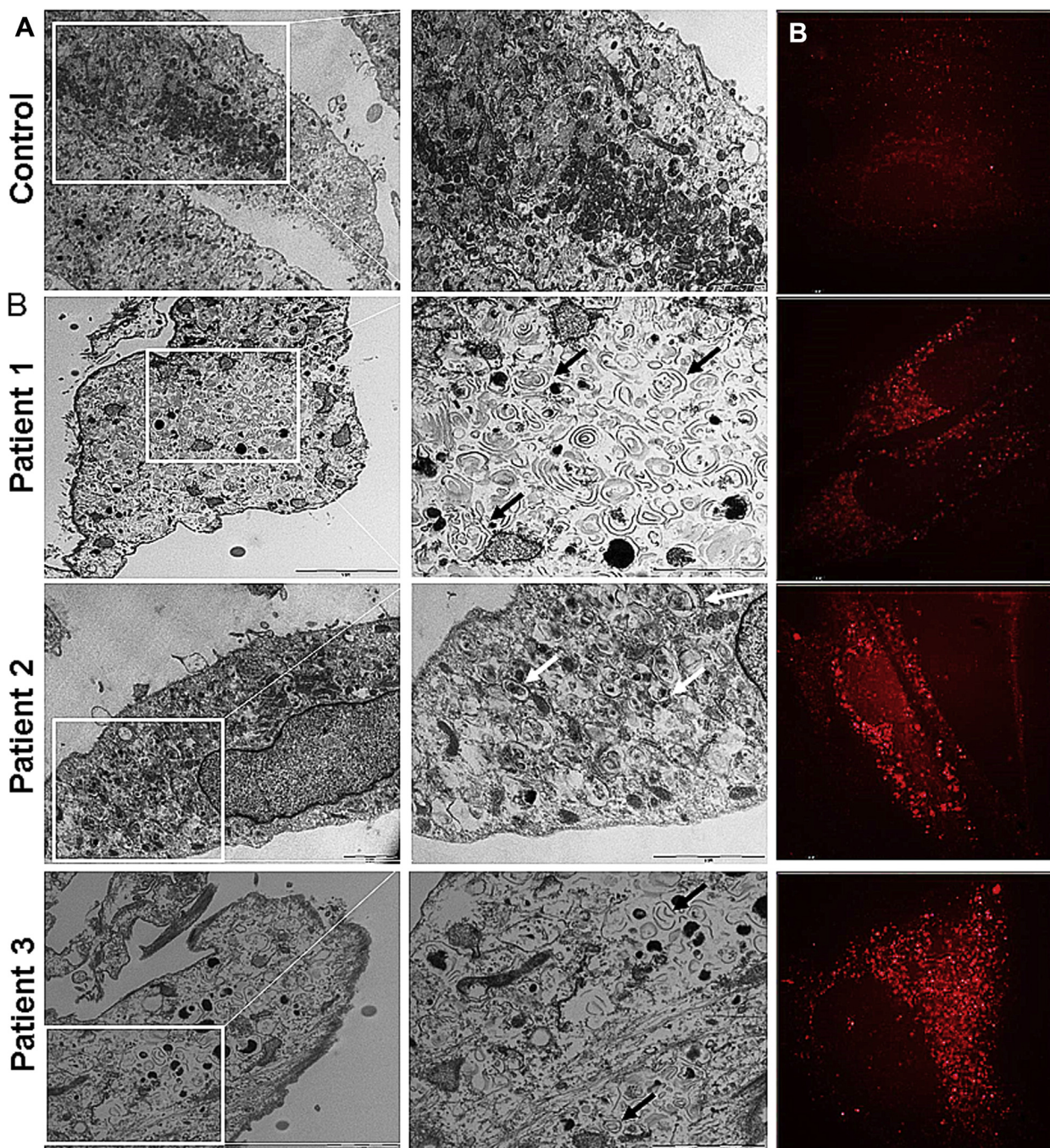


FIG 4. Ultrastructure and LC3 immunofluorescence of fibroblasts from patients with PLS. **A**, Control fibroblasts showing mitochondria with typical ultrastructure with several lamellar bodies (*black arrows*) and autophagosome (*white arrows*) present in fibroblasts from patients with PLS. *Scale bar* = 10 μm (low magnification) and 2 μm (high magnification). **B**, Immunofluorescence of LC3 in cells from control subjects and pathologic cells.

treatment in control cells led to a significant increase in the amount of LC3-II, suggesting normal autophagic flux (Fig 3, B). However, BafA1 treatment in fibroblasts from patients with PLS did not affect LC3-II expression levels, suggesting a defective degradative completion of autophagy (Fig 3, B). Electron microscopy of fibroblasts from patients with PLS confirmed the presence of abundant multilamellar bodies and increased autophagosome numbers, as indicated by the accumulation of double-membrane

vesicle structures (Fig 4, A). Increased expression levels of LC3 in fibroblasts from patients with PLS were also confirmed by using immunofluorescence microscopy (Fig 4, B).

Lysosomal permeability is associated with PLS

Degradation of autophagic substrates takes place in the autophagolysosomal compartment through acidic proteases,

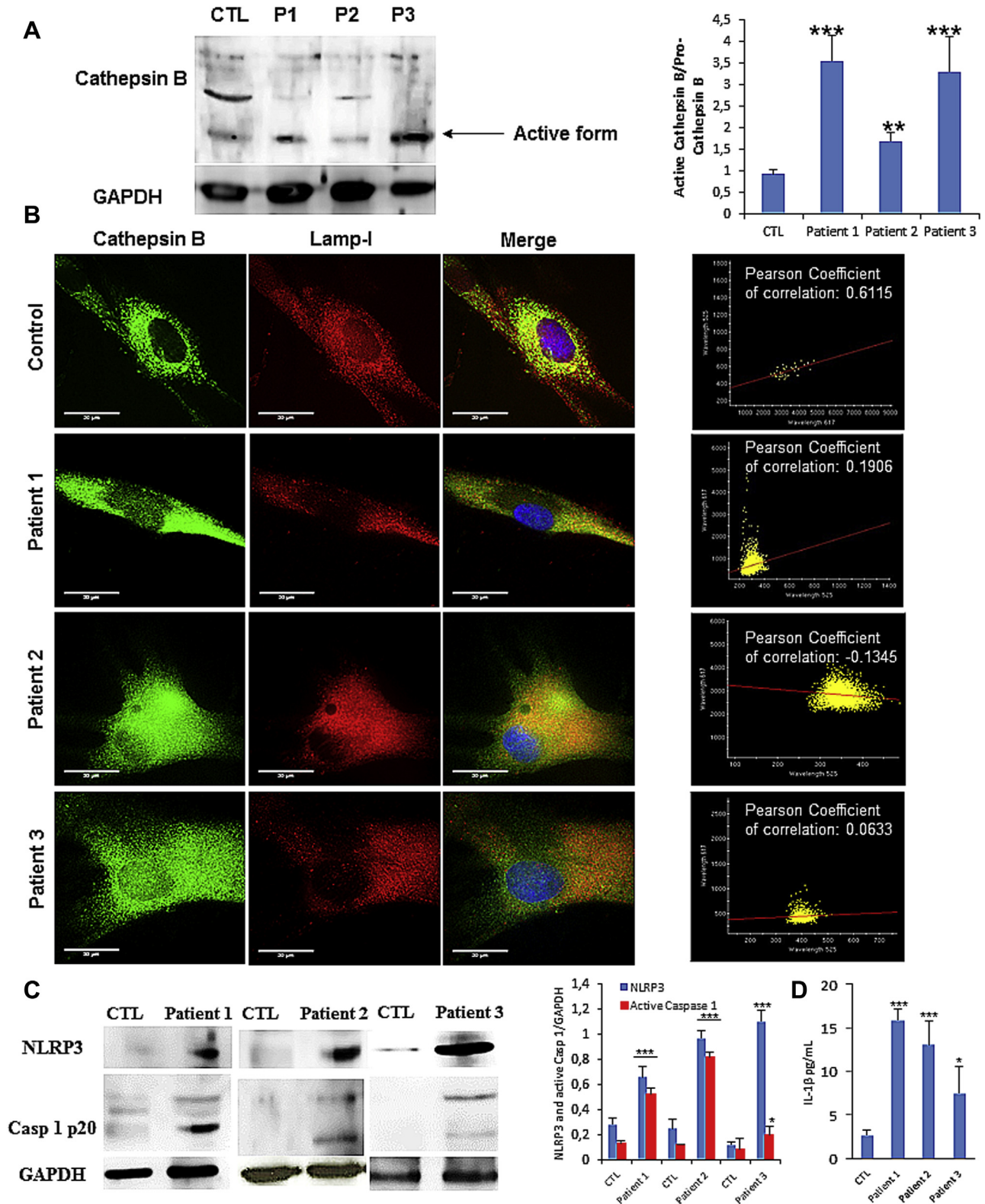


FIG 5. CatB releases in fibroblasts from patients with PLS. **A**, Protein expression levels of CatB were determined in fibroblast cultures from healthy control subjects and patients with PLS by using Western blotting, as described in the Methods section. **B**, Immunofluorescence of CatB in control and pathologic cells. Note that in fibroblasts from patients with PLS, CatB diffuses throughout the cytosol. **C**, NLRP3 inflammasome protein expression levels of NLRP3 (*top band*) and caspase 1 (*intermediate bands*), were determined in fibroblast cultures from healthy control subjects and patients with PLS by using Western blot analysis, as described in the Methods section. Glyceraldehyde-3-phosphate dehydrogenase (*GAPDH*) was used as a loading control. For control cells, data are a pool of 2 different control cell lines. **D**, IL-1 β levels of supernatants from fibroblasts from healthy control subjects and patients with PLS. Data represent mean \pm SDs of 3 separate experiments. * $P < .05$, ** $P < .01$, and *** $P < .001$ between control subjects and patients with PLS.

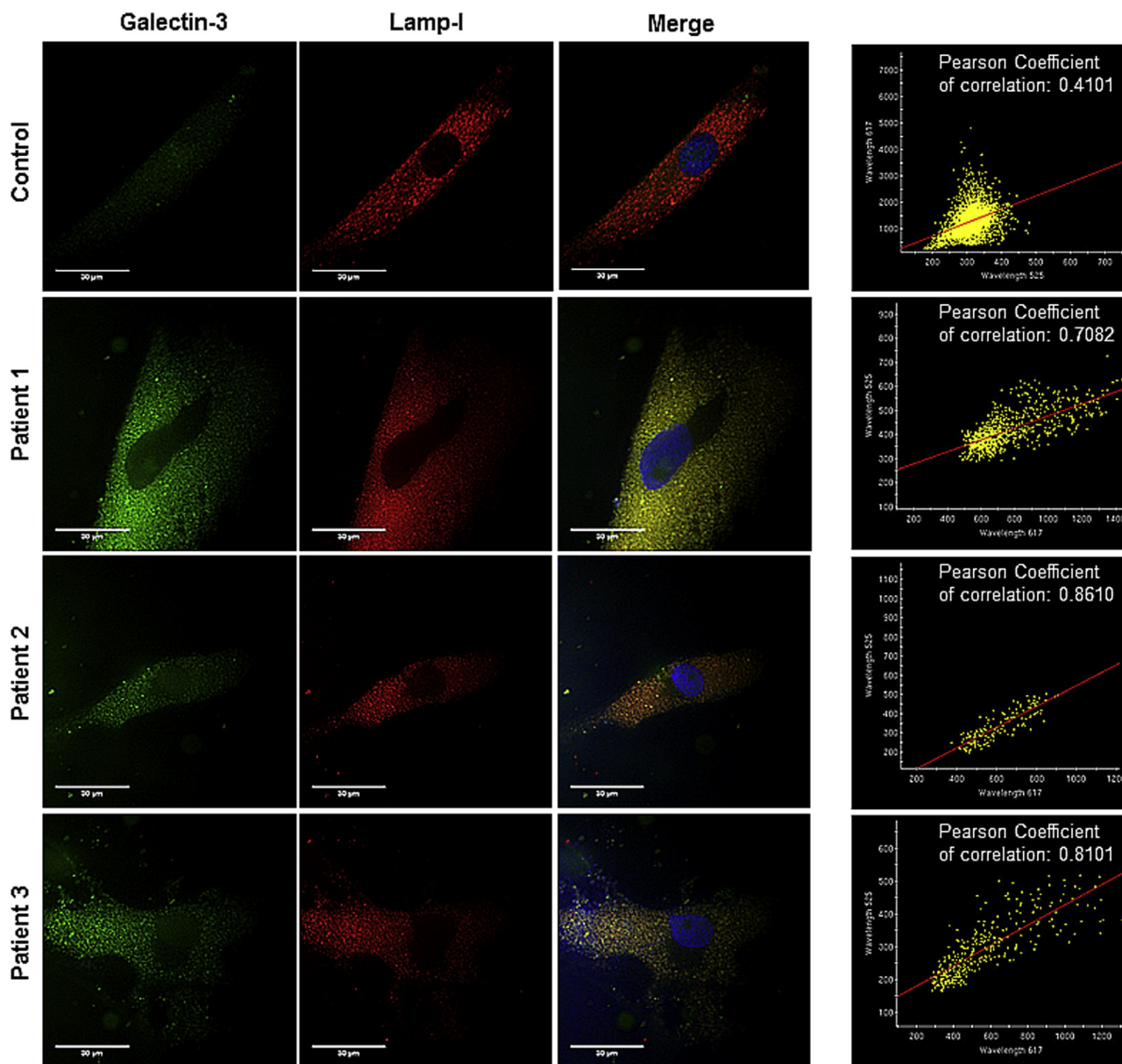


FIG 6. Representative fluorescence images of fibroblasts from control subjects and patients with PLS. Cells were fixed and stained with anti-galectin-3 antibodies (green) and anti-LAMP-1 (red). Nuclei were stained with Hoechst 33342 (blue). Increased galectin-3 puncta and colocalization of galectin-3 and LAMP-1 puncta are shown in patients.

such as cathepsins. Reduced autophagic flux with consequent autophagosome/autophagolysosome accumulation can be a consequence of reduced autophagosome-lysosome fusion or inefficient lysosomal degradation.¹⁸ According to this, we determined whether the impaired autophagic flux in CatC mutant cells was associated secondarily with additional lysosomal dysfunction.

Because the cysteine cathepsin family includes several proteases, such as cathepsins B, C, H, K, and L,¹⁹ we first analyzed expression levels of CatB. Interestingly, active CatB expression levels were increased in fibroblasts from patients with PLS (Fig 5, A). Next, we hypothesized that increased CatB levels might play a central role in the

pathophysiology of PLS through its release from the lysosomal/autophagolysosomal compartment to the cytosol. In healthy fibroblasts CatB signal colocalized with the lysosomal/autophagolysosomal marker LAMP-1, indicating that it was located within lysosomes/autophagolysosomes (Fig 5, B). However, in fibroblasts from patients with PLS, the CatB signal was diffuse through the cytosol and did not colocalize completely with the LAMP-1 marker, suggesting lysosome/autophagolysosome membrane permeabilization (LMP; Fig 5, B). LMP in mutant fibroblasts was also confirmed by detection of galectin puncta at autophagolysosomes (Fig 6), a marker of vacuole lysis, permeabilization, or both.¹⁴ Interestingly, CatB release and lysosomal permeabilization were

accompanied by NLRP3 inflammasome activation assessed by increased expression levels of NLRP3, caspase 1 activation, and pronounced secretion of IL-1 β into culture media (Fig 5, C).

rCatC improves growth rate and induces partial restoration of autophagic flux in mutant fibroblasts

Given that CatC mutations in fibroblasts from patients with PLS induce a marked reduction in the enzymatic activity of CatC, which is associated with impaired autophagic flux and lysosomal dysfunction, we next evaluated the effects of autophagy induction in fibroblasts from patients with PLS using rapamycin treatment, a selective mechanistic target of rapamycin inhibitor. Rapamycin had a moderate effect on LC3 expression levels but no effect on CatB levels or growth rates in fibroblasts from patients with PLS (see Fig E2 in this article's Online Repository at www.jacionline.org).

To examine whether enzyme replacement therapy could be an effective treatment in patients with PLS, we next assessed the effect of rCatC on mutant fibroblasts. rCatC was produced by a baculovirus system in insect cell cultures.²⁰ Enzyme content and activity were tested in both supernatants and cellular insoluble and soluble extracts. Soluble extracts showed the highest enzyme content of rCatC (see Fig E2). Immunoblot analysis of purified rCatC revealed 3 polypeptides with molecular masses of approximately 55, 25, and 7.8 kDa (see Fig E3 in this article's Online Repository at www.jacionline.org). Amounts of 55-kDa polypeptides were much larger than those of the other 2 polypeptides. Flatworm CatC expressed in insect cells also exhibited 3 similar bands of 55-, 25-, and 7.8-kDa polypeptides after purification (see Fig E4 in this article's Online Repository at www.jacionline.org). Enzymatic activity assays showed that the highest enzymatic activity was also found in soluble extracts (see Fig E5 in this article's Online Repository at www.jacionline.org).

Fibroblasts from control subjects and a representative patient with PLS were treated at 3 different doses of rCatC. The results showed a statistically significant dose-dependent reduction of growth rate in fibroblasts from control subjects and patients with PLS (Fig 7, A-C). Enzymatic activity of CatC was partially recovered in the patient's fibroblasts after 120 hours of rCatC treatment (Fig 7, D). Interestingly, rCatC treatment reduced LC3-II and p62/SQSTM1 expression levels, suggesting improvement of autophagic flux in fibroblasts from patients with PLS (Fig 7, E). Additionally, IL-1 β levels in medium were also reduced after rCatC treatment, suggesting decreased inflammasome activation (Fig 7, E).

rCatC improves lysosomal permeability in fibroblasts from patients with PLS

Given that LPM can play a central role in the pathophysiologic alterations found in fibroblasts from patients with PLS, we next evaluated the effects of rCatC treatment on CatB release from lysosomes. Treatment with rCatC induced a marked reduction in CatB expression levels in fibroblasts from patients with PLS (Fig 7, E), as well as an increased colocalization of CatB signal with the LAMP-1 marker, suggesting a reduction of LPM (see Fig E6 in this article's Online Repository at www.jacionline.org). Prevention of LPM after rCatC treatment was also confirmed by the absence of galectin puncta at autophagolysosomes in fibroblasts from patients with PLS (Fig 8).

DISCUSSION

The dearth of knowledge about the molecular basis of PLS leads to a lack of effective therapeutic tools. Previous works have been oriented to the description of new CatC mutations and the description of the pathophysiologic alterations associated with the disease, such as oxidative stress and neutrophil function impairment. The present report provides experimental evidence of metabolic and autophagic impairment in CatC-deficient fibroblasts. First, we assessed metabolic alterations in cultured mutant fibroblasts. As expected, a reduction in mitochondrial bioenergetics was observed. This entailed a significant reduction in cell growth rate in fibroblasts from patients with PLS. Then we provided experimental evidence for the activation of autophagy in CatC-deficient fibroblasts. The autophagic process is initiated by formation of a phagophore or nucleation membrane to which cytoplasmic content is targeted. This phagophore is then elongated, forming an autophagosome, which engulfs material marked for degradation. Finally, mature autophagosomes fuse with lysosomes, resulting in autophagolysosomes, for enzymatic degradation of the cargo.¹⁷ Enhanced autophagy markers might be due to either increased autophagosome formation or impaired clearance of the autophagosomes. Given that the autophagosome is an intermediate structure, the number of autophagosomes observed at any specific time point is the result of the balance between the rate of their generation and the rate of their conversion into autophagolysosomes.

Because LC3-II overexpression can indicate either an increment of autophagy or an impairment of the autophagic flux, LC3-II expression levels must be interpreted together with p62/SQSTM1 expression levels.²¹ Fibroblasts from patients with PLS showed an impaired autophagic flux determined by increased expression levels of both LC3-II and p62/SQSTM1. These results were confirmed by using a BafA1 assay and ultrastructural examination of mutant fibroblasts. Interestingly, defective autophagic degradation activity or autophagic flux occurs in multiple lysosomal diseases, such as Niemann-Pick, Gaucher, and Pompe diseases.²²⁻²⁴

Oxidative stress has been associated previously with the pathophysiology of PLS,² and we observed increased ROS production accompanied by reduced antioxidant defenses in fibroblasts from patients with PLS. Oxidative stress has been implicated in induction of lysosomal instability and membrane permeabilization.²⁵ In addition, a reduction in levels some cysteine cathepsin family members, such as CatL, has been related to a compensatory transcriptional upregulation of CatB expression and autophagy dysfunction.²⁶ Furthermore, in patients with a lysosomal disease, such as Niemann-Pick disease, the increased expression of mature protein forms for both CatB and CatD is associated with autophagosome accumulation.²⁷

Our findings showed reduced enzymatic activity of CatC associated with a compensatory upregulation of mature CatB and lysosomal permeabilization. All these disturbances in the machinery of autophagy and lysosome metabolism could explain several of the clinical phenotypic characteristics of PLS. Thus many patients with PLS show increased susceptibility to infections and periodontal disease.² Given that autophagy plays a key role in the defense mechanism against bacterial infections and autophagic dysfunction has been associated with inflammation and infection progression,⁷ our data could help to better understand this susceptibility. Autophagy is also involved

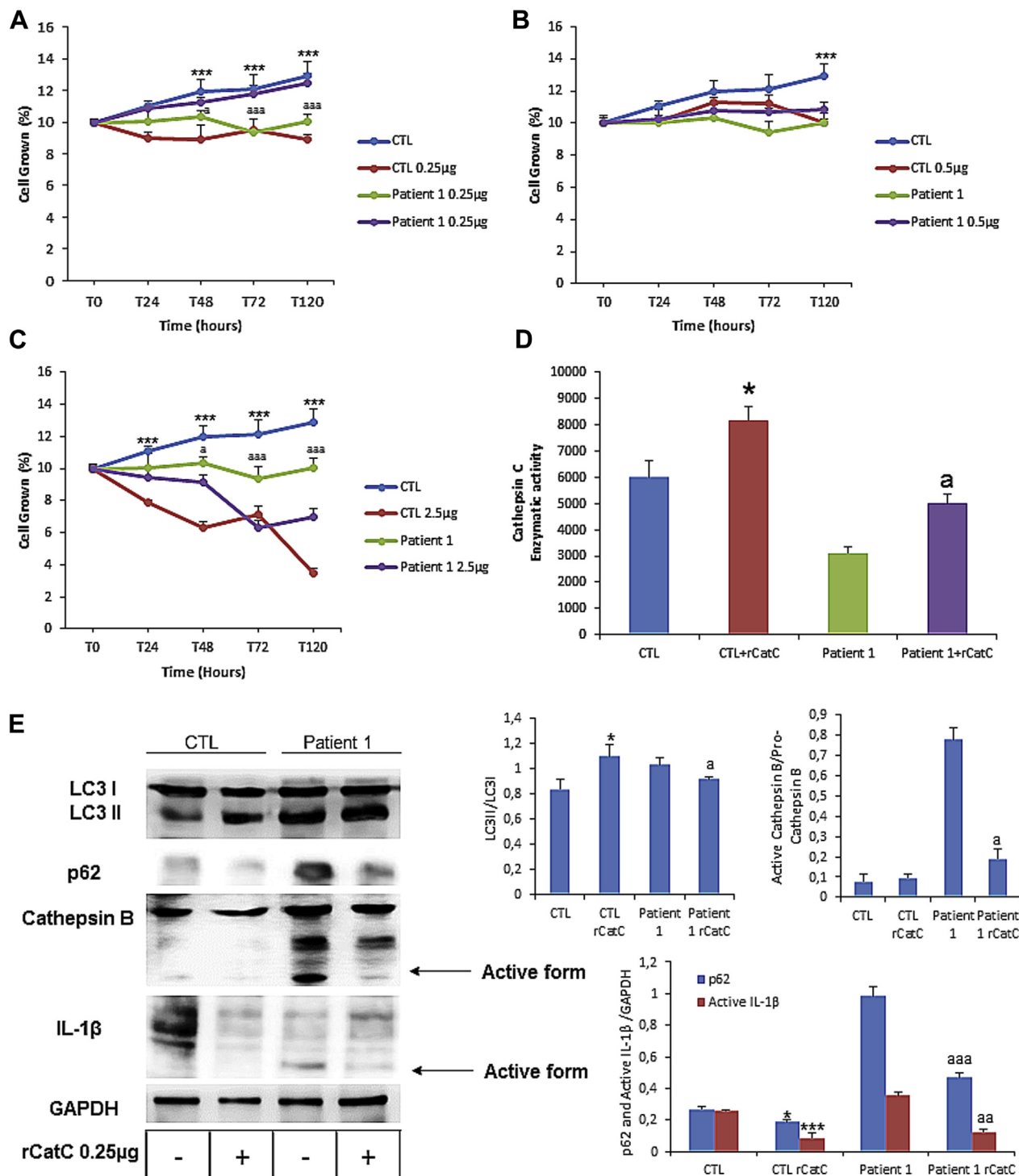


FIG 7. A-C, Cell growth with rCatC levels determined in healthy and representative fibroblasts from patients with PLS. **D**, Enzymatic activity of CatC in homogenates from skin fibroblasts after 120 hours of rCatC treatment. For control cells, data are mean \pm SDs for experiments conducted on 2 different control cell lines. Data represent mean - SDs of 3 separate experiments. * $P < .01$ between control subjects and control subjects treated with rCatC. ^a $P < .01$ between patients with PLS and patients with PLS treated with rCatC. **E**, Autophagic protein expression levels of LC3 and p62, CatB, and IL-1 β were determined in control and representative PLS fibroblast cultures after rCatC treatment by using Western blot analysis, as described in the Methods section. For control cells, data are means \pm SDs for experiments conducted on 2 different control cell lines. Glyceraldehyde-3-phosphate dehydrogenase (*GAPDH*) was used as a loading control. For control cells in Western blots, data are a pool of 2 different control cell lines. * $P < .05$, *** $P < .001$ between control subjects and control subjects treated with rCatC. ^{aa} $P < .05$, ^{aaa} $P < .001$ between patients with PLS and patients with PLS treated with rCatC.

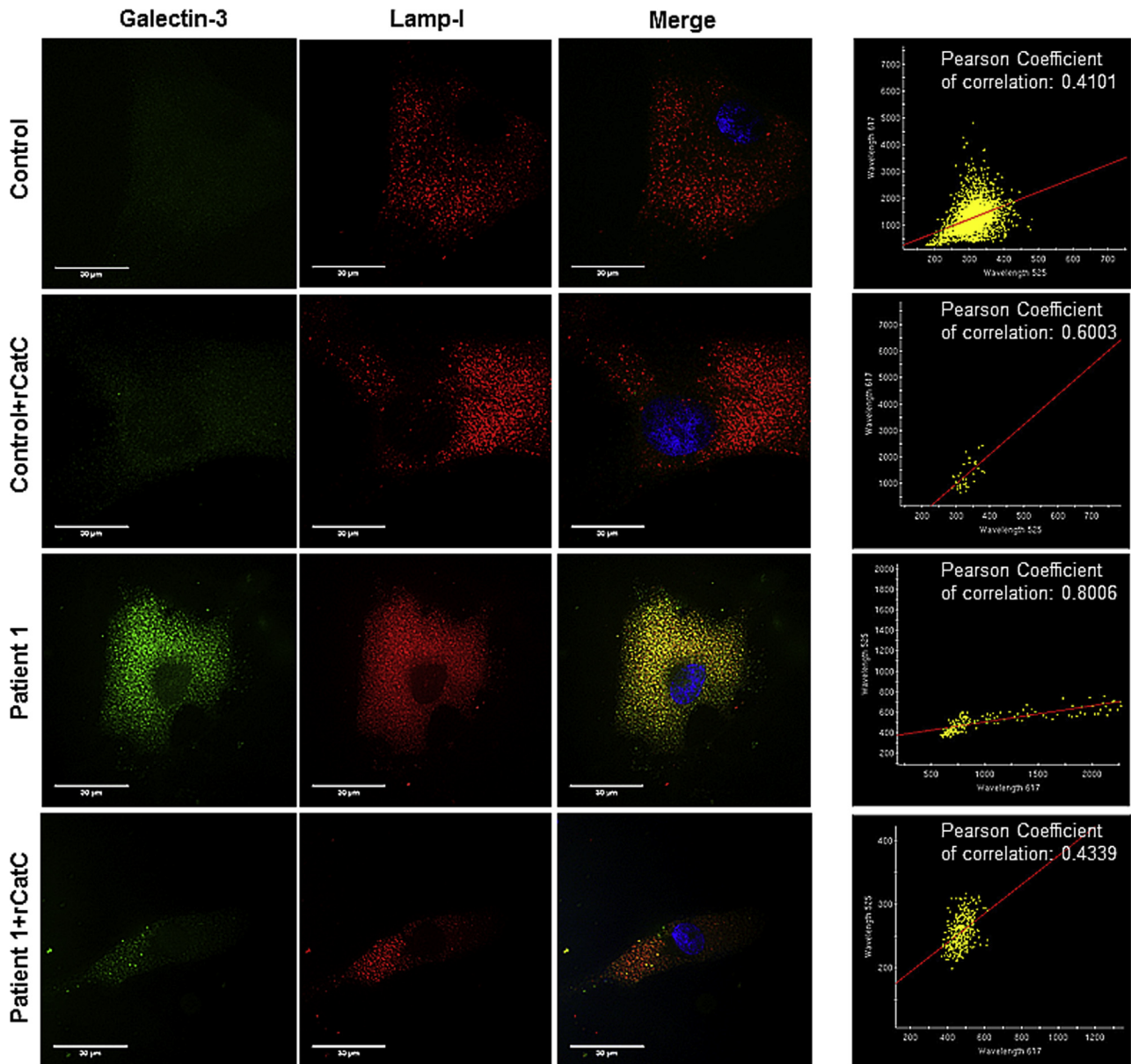


FIG 8. Representative fluorescence images of fibroblasts from control subjects and patients with PLS to evaluate the effect of rCatC in lysosomal permeabilization. Cells were fixed and stained with anti-galectin-3 antibodies (green) and anti-LAMP-1 (red). Nuclei were stained with Hoechst 33342 (blue). Increased galectin-3 puncta and colocalization of galectin-3 and LAMP-1 puncta are shown in patients.

in skin homeostasis, which is the first line of defense against many different insults. However, the exact mechanism by which autophagy dysfunction could be involved in the development of skin diseases is still unknown. Nevertheless, several skin disorders, such as vitiligo, psoriasis, hyperpigmentation, or the skin alterations seen in patients with systemic lupus erythematosus, have been related to autophagy defects.²⁸ In addition, autophagy dysregulation can lead to p62/SQSTM1-dependent inflammatory cytokine production, as has been reported for psoriatic skin.²⁹ In the present study we found a similar autophagy dysfunction associated with p62/SQSTM1 accumulation, NLRP3 inflammasome activation, and increased production of inflammatory cytokines. Inflammasome complexes are activated by a wide variety

of danger signals, including release of cathepsins into the cytosol after lysosomal destabilization.³⁰ Therefore the inflammatory profile of PLS could be explained by CatB release from lysosomes and subsequent NLRP3 inflammasome activation.

According to our study, autophagic dysfunction had a relevant role in PLS pathophysiology, but autophagy modulation by rapamycin has not been demonstrated to improve the cells, probably showing a more relevant role of CatB in the pathophysiology of PLS, which was not reduced by rapamycin treatment.

Our data obtained in a fibroblast cell model can be useful for understanding the pathologic alterations of skin. Given the important role of autophagy in many tissue and cell types, other

pathologic effects could be observed in patients with PLS. For example, autophagic dysfunction in long-lived cells, such as neurons and podocytes, could induce clinical symptoms in the central nervous system or kidneys in patients with PLS. However, we have no evidence of these clinical manifestations, in part because there are no complete long-term follow-up studies of patients with PLS and the clinical description is limited to single cases. Recently, a T-cell immunodeficiency phenotype was shown in patients with PLS.⁷ Because T and B cells have the same origin, the lymphoblast, this finding could suggest that long-lived plasma cells could be involved also in the molecular bases of PLS and could involve other cellular models.

Finally, the treatment and management of PLS is poor and limited to oral and dermatologic treatments with emollients, salicylic acid, and topical steroids, which are often accompanied by toxic effects.³¹ Therefore it is important to develop effective pharmacologic treatments for PLS targeting the underlying molecular pathways of the disease. Accordingly, we designed an enzyme replacement therapy strategy to correct pathophysiologic markers in fibroblasts from patients with PLS. Enzyme replacement therapies have now been accepted as an effective approach in patients with several lysosomal diseases.³² Thus we treated fibroblasts from patients with PLS with rCatC produced in insect cells. Treatment with rCatC corrected autophagy dysfunction, reduced LPM, and improved cell growth rates. To the best of our knowledge, for the first time, this study shows new molecular pathways and pharmacologic targets in patients with PLS. Furthermore, rCatC can be an interesting therapeutic approach for the treatment of CatC deficiency in patients with PLS.

We thank Ms Monica Glebocki for extensive editing of the manuscript.

Key messages

- Patients with PLS show autophagic and lysosomal dysfunction.
- CatB release induces NLRP3 inflammasome activation in patients with PLS.
- rCatC could benefit PLS treatment.

REFERENCES

1. Roberts H, White P, Dias I, McKaig S, Veeramachaneni R, Thakker N, et al. Characterization of neutrophil function in Papillon-Lefèvre syndrome. *J Leukoc Biol* 2016;100:433-44.
2. Bullón P, Morillo JM, Thakker N, Veeramachaneni R, Quiles JL, Ramírez-Tortosa MC, et al. Confirmation of oxidative stress and fatty acid disturbances in two further Papillon-Lefèvre syndrome families with identification of a new mutation. *J Eur Acad Dermatol Venereol* 2014;28:1049-56.
3. Guarino C, Hamon Y, Croix C, Lamort AS, Dallet-Choisy S, Marchand-Adam S, et al. Prolonged pharmacological inhibition of cathepsin C results in elimination of neutrophil serine proteases. *Biochem Pharmacol* 2017;131:52-67.
4. Sørensen OE, Clemmensen SN, Dahl SL, Østergaard O, Heegaard NH, Glenthøj A, et al. Papillon-Lefèvre syndrome patient reveals species-dependent requirements for neutrophil defenses. *J Clin Invest* 2014;124:4539-48.
5. Méthot N, Rubin J, Guay D, Beaulieu C, Ethier D, Reddy TJ, et al. Inhibition of the activation of multiple serine proteases with a cathepsin C inhibitor requires sustained exposure to prevent pro-enzyme processing. *J Biol Chem* 2007;282:20836-46.
6. Pham CT, Ivanovich JL, Raptis SZ, Zehnauer B, Ley TJ. Papillon-Lefèvre syndrome: correlating the molecular, cellular, and clinical consequences of cathepsin C/dipeptidyl peptidase I deficiency in humans. *J Immunol* 2004;173:7277-81.
7. Yin Z, Pascual C, Klionsky DJ. Autophagy: machinery and regulation. *Microb Cell* 2016;3:588-96.
8. Koike M, Shibata M, Waguri S, Yoshimura K, Tanida I, Kominami E, et al. Participation of autophagy in storage of lysosomes in neurons from mouse models of neuronal ceroid-lipofuscinoses (Batten disease). *Am J Pathol* 2005;167:1713-28.
9. Settembre C, Fraldi A, Rubinsztein DC, Ballabio A. Lysosomal storage diseases as disorders of autophagy. *Autophagy* 2008;4:113-4.
10. Tatti M, Motta M, Di Bartolomeo S, Cianfanelli V, Salvioli R. Cathepsin-mediated regulation of autophagy in saposin C deficiency. *Autophagy* 2013;9:241-3.
11. Hewitt C, McCormick D, Linden G, Turk D, Stern I, Wallace I, et al. The role of cathepsin C in Papillon-Lefèvre syndrome, prepubertal periodontitis, and aggressive periodontitis. *Hum Mutat* 2004;23:222-8.
12. Aebi H. Catalase in vitro. *Methods Enzymol* 1984;105:121-6.
13. Kakkar P, Das B, Viswanathan PN. A modified spectrophotometric assay of superoxide dismutase. *Indian J Biochem Biophys* 1984;21:130-2.
14. Aits S, Krieger J, Liu B, Ellegaard AM, Hamalissi S, Tvingsholm S, et al. Sensitive detection of lysosomal membrane permeabilization by lysosomal galectin puncta assay. *Autophagy* 2015;11:1408-24.
15. Lefèvre C, Blanchet-Bardon C, Jobard F, Bouadjar B, Stalder JF, Cure S, et al. Novel point mutations, deletions, and polymorphisms in the cathepsin C gene in nine families from Europe and North Africa with Papillon-Lefèvre syndrome. *J Invest Dermatol* 2001;117:1657-61.
16. Hart PS, Zhang Y, Firatli E, Uygur C, Lotfazar M, Michalec MD, et al. Identification of cathepsin C mutations in ethnically diverse Papillon-Lefèvre syndrome patients. *J Med Genet* 2000;37:927-32.
17. Codogno P. Shining light on autophagy. *Nat Rev Mol Cell Biol* 2014;15:153.
18. Mizushima N, Levine B, Cuervo AM, Klionsky DJ. Autophagy fights disease through cellular self-digestion. *Nature* 2008;451:1069-75.
19. Kaminsky V, Zhivotovsky B. Proteases in autophagy. *Biochim Biophys Acta* 2012;1824:44-50.
20. Qiu GF, Feng HY, Yamano K. Expression and purification of active recombinant cathepsin C (dipeptidyl aminopeptidase I) of kuruma prawn *Marsupenaeus japonicus* in insect cells. *J Biomed Biotechnol* 2009;2009:746289.
21. Klionsky DJ, Abdelmohsen K, Abe A, Abedin MJ, Abeliovich H, Acevedo Arozana A, et al. Guidelines for the use and interpretation of assays for monitoring autophagy (3rd edition). *Autophagy* 2016;12:1-222.
22. Guo H, Zhao M, Qiu X, Deis JA, Huang H, Tang QQ, et al. Niemann-Pick type C2 deficiency impairs autophagy-lysosomal activity, mitochondrial function, and TLR signaling in adipocytes. *J Lipid Res* 2016;57:1644-58.
23. Aflaki E, Moaven N, Borger DK, Lopez G, Westbroek W, Chae JJ, et al. Lysosomal storage and impaired autophagy lead to inflammasome activation in Gaucher macrophages. *Aging Cell* 2016;15:77-88.
24. Spanpanato C, Feeney E, Li L, Cardone M, Lim JA, Annunziata F, et al. Transcription factor EB (TFEB) is a new therapeutic target for Pompe disease. *EMBO Mol Med* 2013;5:691-706.
25. Boya P, Kroemer G. Lysosomal membrane permeabilization in cell death. *Oncogene* 2008;27:6434-51.
26. Mizunoe Y, Sudo Y, Okita N, Hiraoka H, Mikami K, Narahara T, et al. Involvement of lysosomal dysfunction in autophagosome accumulation and early pathologies in adipose tissue of obese mice. *Autophagy* 2017;13:642-53.
27. Liao G, Yao Y, Liu J, Yu Z, Cheung S, Xie A, et al. Cholesterol accumulation is associated with lysosomal dysfunction and autophagic stress in Npc1 ^{-/-} mouse brain. *Am J Pathol* 2007;171:962-75.
28. Yu T, Zuber J, Li J. Targeting autophagy in skin diseases. *J Mol Med (Berl)* 2015;93:31-8.
29. Lee HM, Shin DM, Yuk JM, Shi G, Choi DK, Lee SH, et al. Autophagy negatively regulates keratinocyte inflammatory responses via scaffolding protein p62/SQSTM1. *J Immunol* 2011;186:1248-58.
30. Guo H, Callaway JB, Ting JP. Inflammasomes: mechanism of action, role in disease, and therapeutics. *Nat Med* 2015;21:677-87.
31. Sreeramulu B, Shyam ND, Ajay P, Suman P. Papillon-Lefèvre syndrome: clinical presentation and management options. *Clin Cosmet Investig Dent* 2015;7:75-81.
32. Wyatt K, Henley W, Anderson L, Anderson R, Nikolaou V, Stein K, et al. The effectiveness and cost-effectiveness of enzyme and substrate replacement therapies: a longitudinal cohort study of people with lysosomal storage disorders. *Health Technol Assess* 2012;16:1-543.

METHODS**WT sequence of CatC**

MGAGPSLLLAALLLLLSGDGAVRCDTPANCTYLDLLGTWVFVQG
SSGSQRDVNCSVMGPQ
EKKVVVYLQKLDTAYDDLGN SGHFTHIYNQGFIVLNDYKWFAFF
KYKEEGSKVTTYCNE
TMTGWVHDVLDGRNWACFTGKKVGTASENVVYVNI AHLKNSQEKY
SNRLYKYDHNFKAINA
IQKSWTATTYMEYETLTLGDMIRRS GGHSR KIPRKPAPLTA EIQQ
KILHLPTS WDWRNV
HGINFVSPVRNQASCGSCYSFASMGMLEARIRILTNN SQTPILSPQE
VVSCSQYAQGCEG
GFPYLIAGKYAQDFGLVEEACFPYTGTDS PCKMKEDCFRYSSEY
HYVGGFYGGCNEALM
KLELVHHGPM AVAFEVYDDFLHYKKG IYHHTGLRDPFNP FELTNH
AVLLVGYG TDSASGM
DYWIVKNSWGTGWGENGYFRIRRG TDECAIESIAVAATPIPKL.

Patient 1: p.Y32* (lost sequence by a premature stop codon is shown in boldface)

MGAGPSLLLAALLLLLSGDGAVRCDTPANCTYLDLLGTWVFVQG
SSGSQRDVNCSVMGPQ
EKKVVVYLQKLDTAYDDLGN SGHFTHIYNQGFIVLNDYKWFA
FFKYKEEGSKVTTYCNE
TMTGWVHDVLDGRNWACFTGKKVGTASENVVYVNI AHLKNSQE
KYSNRLYKYDHNFKAINA
IQKSWTATTYMEYETLTLGDMIRRS GGHSR KIPRKPAPLTA E
IQKILHLPTS WDWRNV
HGINFVSPVRNQASCGSCYSFASMGMLEARIRILTNN SQTPILS
PQEVVSCSQYAQGCEG
GFPYLIAGKYAQDFGLVEEACFPYTGTDS PCKMKEDCFRYSSEY
SEYHYVGGFYGGCNEALM
KLELVHHGPM AVAFEVYDDFLHYKKG IYHHTGLRDPFNP FEL
TNHAVLLVGYG TDSASGM
DYWIVKNSWGTGWGENGYFRIRRG TDECAIESIAVAATPIPKL
Wild-type: TAT
Mutant: TAG

Patient 1: p.W134*

MGAGPSLLLAALLLLLSGDGAVRCDTPANCTYLDLLGTWVFVQG
SSGSQRDVNCSVMGPQ
EKKVVVYLQKLDTAYDDLGN SGHFTHIYNQGFIVLNDYKWFAFF
KYKEEGSKVTTYCNE
TMTGWVHDVLDGRNWACFTGKKVGTASENVVYVNI AHLKNSQE
KYSNRLYKYDHNFKAINA
IQKSWTATTYMEYETLTLGDMIRRS GGHSR KIPRKPAPLTA E
IQKILHLPTS WDWRNV

HGINFVSPVRNQASCGSCYSFASMGMLEARIRILTNN SQTPILS
PQEVVSCSQYAQGCEG
GFPYLIAGKYAQDFGLVEEACFPYTGTDS PCKMKEDCFRYSSEY
EYHYVGGFYGGCNEALM
KLELVHHGPM AVAFEVYDDFLHYKKG IYHHTGLRDPFNP FEL
TNHAVLLVGYG TDSASGM
DYWIVKNSWGTGWGENGYFRIRRG TDECAIESIAVAATPIPKL
Wild-type: TGG
Mutant: TAA

Patient 2

MGAGPSLLLAALLLLLSGDGAVRCDTPANCTYLDLLGTWVFVQG
SSGSQRDVNCSVMGPQ
EKKVVVYLQKLDTAYDDLGN SGHFTHIYNQGFIVLNDYKWFAFF
KYKEEGSKVTTYCNE
TMTGWVHDVLDGRNWACFTGKKVGTASENVVYVNI AHLKNSQEKY
SNRLYKYDHNFKAINA
IQKSWTATTYMEYETLTLGDMIRRS GGHSR KIPRKPAPLTA EIQQ
KILHLPTS WDWRNV
HGINFVSPVRNQASCGSCYSFASMGMLEARIRILTNN SQTPILSPQE
VVSCSQYAQGCEG
GFPYLIAGKYAQDFGLVEEACFPYTGTDS PCKMKEDCFRYSSEY
HYVGGFYGGCNEALM
KLELVHHGPM AVAFEVYDDFLHYKKG IYHHTGLRDPFNP FELTNH
AVLLVGYG TDSASGM
DYWIVKNSWGTGWGENGYFRIRRG TDECAIESIAVAATPIPKL
Wild-type: TGG
Mutant: TAA

Patient 3 (the new sequence that is generated is shown in boldface, until reaching the premature STOP)

MGAGPSLLLAALLLLLSGDGAVRCDTPANCTYLDLLGTWVFVQG
SSGSQRDVNCSVMGPQ
EKKVVVYLQKLDTAYDDLGN SGHFTHIYNQGFIVLNDYKWFAFF
KYKEEGSKVTTYCNE
TMTGWVHDVLDGRNWACFTGKKVGTASENVVYVNI AHLKNSQEKY
SNRLYKYDHNFKAINA
IQKSWTATTYMEYETLTLGDMIRRS GGHSR KIPRKPAPLTA EIQQ
KILHLPTS WDWRNV
HGINFVSPVRNQASCGSCYSFASMGMLEARIRILTNN SQTPILSPQE
VVSCSQYAQGCEG
GFPYLIAGKYAQDFGLVEEACFPYTGTDS PCKMKEDCFRYSSEY
HYVGGFYGGCNEALM
KLELVHHGPM AVAFEVYDDF**STTKRGSTTLV**
Wild-type: TTCTCCACTAC...
Mutant: TTCTCCACTAC...

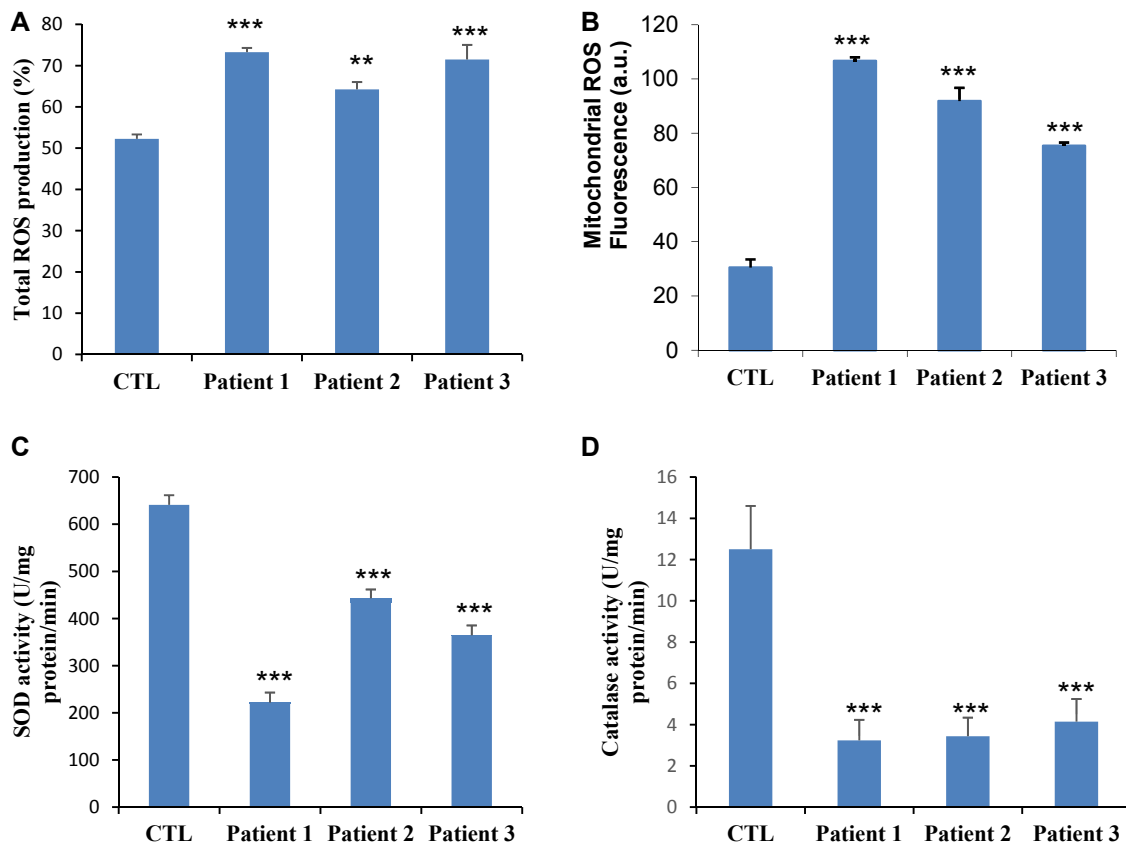


FIG E1. Oxidative stress and oxidative damage levels in fibroblasts from patients with PLS. **A** and **B**, Total and mitochondrial ROS production was analyzed in fibroblasts from control subjects and patients with PLS by using flow cytometry, as described in the Methods section. **C** and **D**, Activities of the antioxidant enzymes superoxide dismutase (*SOD*) and catalase activities were also analyzed in fibroblasts from control subjects and patients with PLS, as described in the Methods section. Data represent means \pm SDs of 3 separate experiments. ** $P < .01$ and *** $P < .001$ between control subjects and patients with PLS.

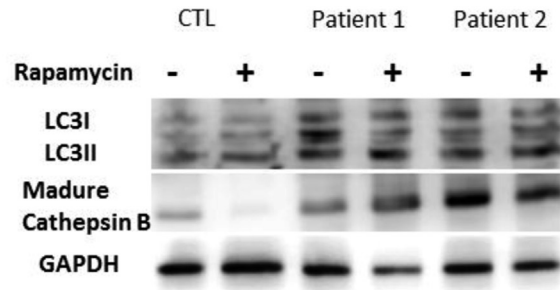
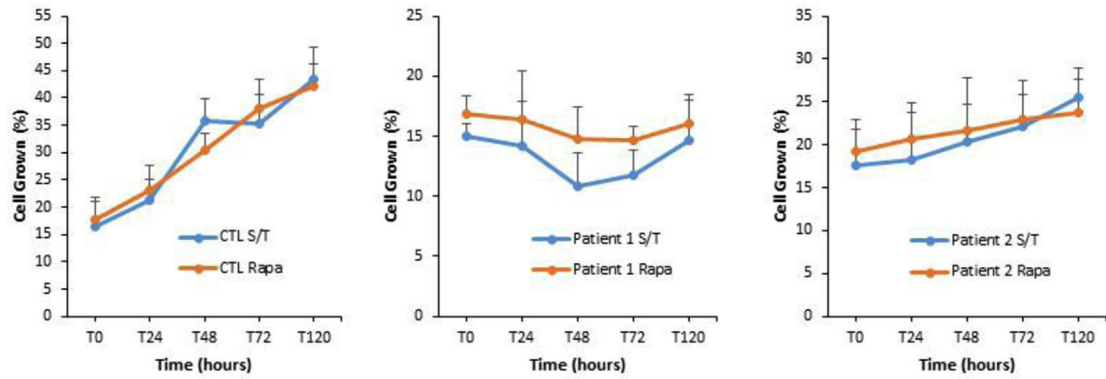
A**B**

FIG E2. Effect of autophagy induction by rapamycin treatment. **A**, LC3 and CatB levels were determined in fibroblast cultures from healthy control subjects and patients with PLS by using Western blot analysis, as described in the Methods section. **B**, Cell growth was determined in fibroblasts from healthy control subjects and patients with PLS.

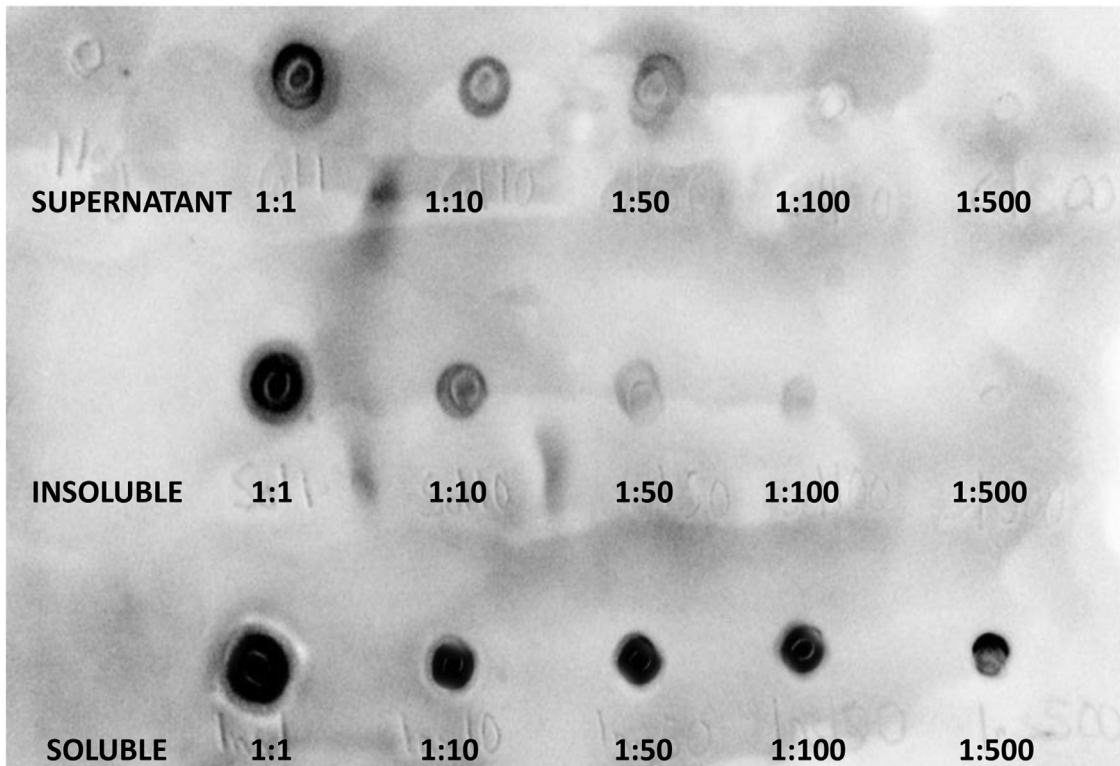


FIG E3. Detection of CatC protein in 2 different extracts (supernatant and soluble and insoluble extracts) determined by using dot blotting.

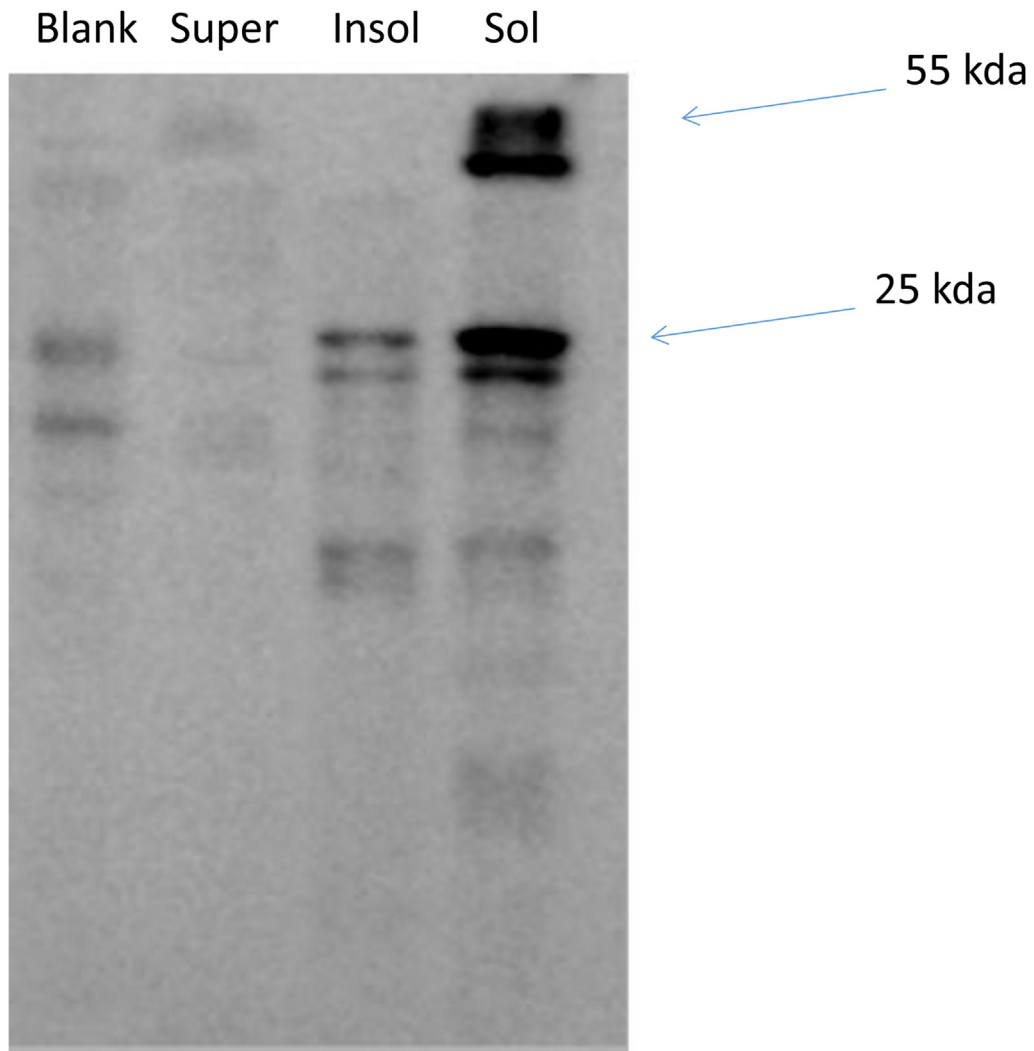


FIG E4. Immunoblot analysis of the insoluble extract revealed 3 polypeptides with molecular masses of approximately 55, 25, and 7.8 kDa. *Insol*, Insoluble; *Sol*, soluble; *Super*, supernatant.

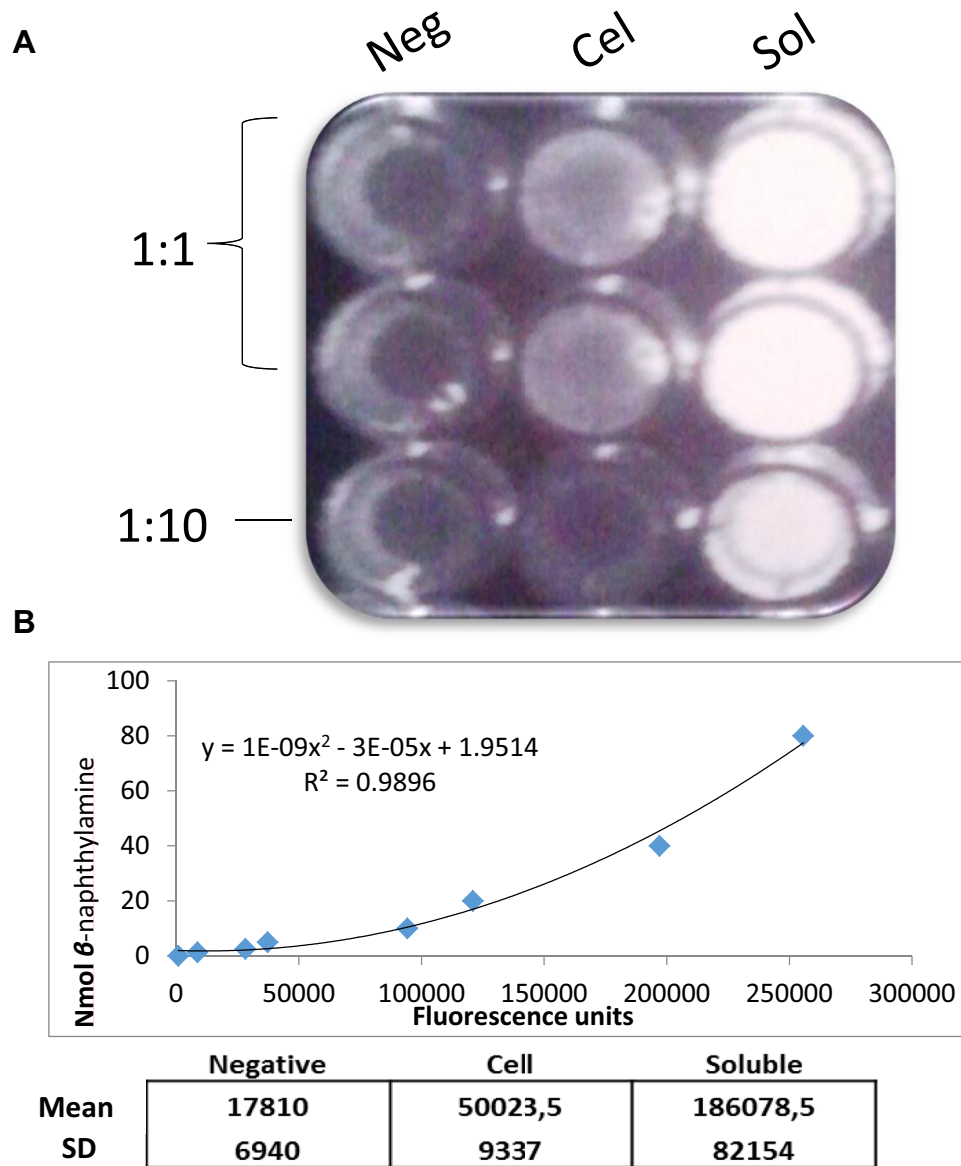


FIG E5. Enzymatic activity of cellular (*Cel*) and soluble (*Sol*) extracts. **A**, Image capture of the assay with the extract. **B**, Quantification curve of the enzymatic activity.

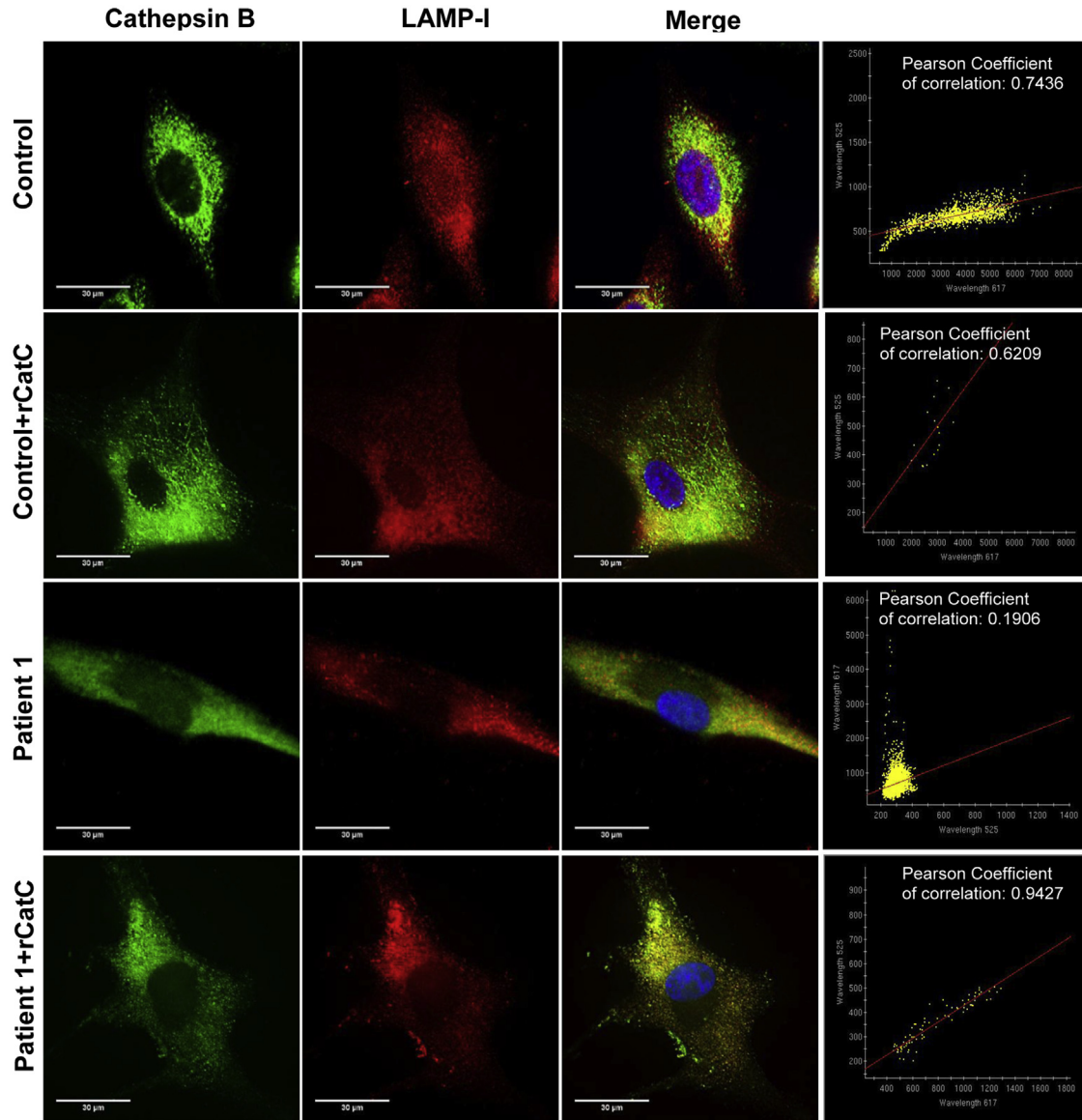


FIG E6. Representative fluorescence images of fibroblasts from healthy control subjects and patients with PLS with and without rCatC treatment. Cells were fixed and stained with anti-CatB antibodies (green) and anti-LAMP-1 (red). Nuclei were stained with Hoechst 33342 (blue). Note that in fibroblasts from patients with PLS, CatB diffuses throughout the cytosol, and increased colocalization with LAMP-1 is observed after rCatC treatment in patients' cells.